Further Pharmacological and Genetic Evidence for the Efficacy of PlGF Inhibition in Cancer and Eye Disease

Sara Van de Veire,[1,2,3,18] Ingeborg Stalmans,[3,18] Femke Heindryckx,[4,18] Hajimu Oura,[5,18] Annemilaï Tijeras-Raballand,[6,18] Thomas Schmidt,[1,2,18] Sonja Loges,[1,2] Imke Albrecht,[7] Bart Jonckx,[1,2] Stefan Vinckier,[1,2] Christophe Van Steenkiste,[4] Sònia Tugues,[8,9] Charlotte Rolny,[9] Maria De Mol,[1,2] Daniela Dettori,[1,2] Patricia Hainaud,[6] Lieve Coenegrachts,[10] Jean-Olivier Contreres,[6] Tine Van Bergen,[3] Henar Cuervo,[1,2] Wei-Hong Xiao,[11] Carole Le Henaff,[6] Ian Buysschaert,[1,2] Behzad Kharabi Masouleh,[1,2] Anja Geerts,[4] Tibor Schomber,[7] Philippe Bonnin,[6] Vincent Lambert,[12] Jurgen Haustraete,[13] Serena Zacchigna,[14] Jean-Marie Rakic,[12] Wladimiro Jiménez,[8,15] Agnes Noël,[12] Mauro Giacca,[14] Isabelle Colle,[4] Jean-Michel Foidart,[12] Gerard Tobelem,[6] Manuel Morales-Ruiz,[8] José Vilar,[16] Patrick Maxwell,[17] Stanley A. Vinores,[1,2,11] Geert Carmeliet,[10] Mieke Dewerchin,[1,2] Lena Claesson-Welsh,[9] Evelyne Dupuy,[6] Hans Van Vlierberghe,[4] Gerhard Christofori,[7] Massimiliano Mazzone,[1,2] Michael Detmar,[5] Désiré Collen,[1,2] and Peter Carmeliet[1,2,*]

[1]Vesalius Research Center, K.U. Leuven, Leuven B-3000, Belgium
[2]Vesalius Research Center, VIB, Leuven B-3000, Belgium
[3]Laboratory of Ophthalmology, K.U. Leuven, Leuven B-3000, Belgium
[4]Department of Gastroenterology & Hepatology, University Hospital, Ghent B-9000, Belgium
[5]Institute of Pharmaceutical Sciences, ETH Zurich CH-8057, Switzerland
[6]Institut des vaisseaux & du sang, angiogenèse et recherche translationelle, Inserm U965, Paris, France
[7]Institute for Biochemistry and Genetics, University of Basel, Basel 4051, Switzerland
[8]Biochemistry and Molecular Genetics Service, IDIBAPS, Hospital Clínic of Barcelona, CIBEREHD, University of Barcelona, Barcelona 08036, Spain
[9]Department of Genetics & Pathology, Rudbeck Laboratory, Uppsala University, 751 85 Uppsala, Sweden
[10]Laboratory of Experimental Medicine & Endocrinology, K.U. Leuven, Leuven B-3000, Belgium
[11]Wilmer Eye Institute, Johns Hopkins University, Baltimore, MD 21218, USA
[12]Laboratory of Tumour & Development Biology, GIGA-Cancer, University of Liège, Liège B-4000, Belgium
[13]Protein service facility, VIB, Ghent B-9052, Belgium
[14]Molecular Medicine, International Centre Genetic Engineering & Biotechnology, Trieste 34149, Italy
[15]Department of Physiology, University of Barcelona 08036, Spain
[16]Cardiovascular Research Center, INSERM U970, Hôpital Européen Georges Pompidou, Université Paris 5, France
[17]UCL Division of Medicine, The Rayne Institute, London WC1E 6JF, UK
[18]These authors contributed equally to this work
*Correspondence: peter.carmeliet@vib-kuleuven.be
DOI 10.1016/j.cell.2010.02.039

SUMMARY

Our findings that PlGF is a cancer target and anti-PlGF is useful for anticancer treatment have been challenged by Bais et al. Here we take advantage of carcinogen-induced and transgenic tumor models as well as ocular neovascularization to report further evidence in support of our original findings of PlGF as a promising target for anticancer therapies. We present evidence for the efficacy of additional anti-PlGF antibodies and their ability to phenocopy genetic deficiency or silencing of PlGF in cancer and ocular disease but also show that not all anti-PlGF antibodies are effective. We also provide additional evidence for the specificity of our anti-PlGF antibody and experiments to suggest that anti-PlGF treatment will not be effective for all tumors and why. Further, we show that PlGF blockage inhibits vessel abnormalization rather than density in certain tumors while enhancing VEGF-targeted inhibition in ocular disease. Our findings warrant further testing of anti-PlGF therapies.

INTRODUCTION

Placental growth factor (PlGF) is a VEGF homolog. Studies in independently generated *PlGF*$^{-/-}$ lines identified a role for PlGF in ischemic, inflammatory, and malignant disease (Carmeliet et al., 2001; E. Cheung et al., IOVS 2009;50:ARVO E-Abstract 2943; Fischer et al., 2008; Luttun et al., 2002a; Van Steenkiste et al., 2009). PlGF induces responses in endothelial, malignant, immune, and other cells and binds to Flt1 (Fischer et al., 2008). Although Flt1 may act as a trap for VEGF, it also transmits signals in response to PlGF via its tyrosine kinase (TK) domains (Landgren et al., 1998). The role of Flt1 in cancer remains controversial, but most studies report that Flt1 inhibition/silencing reduces tumor growth in preclinical models. In mice expressing Flt1 without TK activity (*Flt1-TK*$^{-/-}$), tumor growth and metastasis

are inhibited (Hiratsuka et al., 2002) or not affected (Dawson et al., 2009).

Clinical studies show that PlGF levels correlate with poor prognosis of various cancers, including hepatocellular, colorectal, renal, and other cancers (Fischer et al., 2008; Ho et al., 2006), though PlGF is also epigenetically silenced (Xu and Jain, 2007). PlGF levels are upregulated in cancer patients treated with VEGF inhibitors (Willett et al., 2005). Moreover, PlGF expression in tumor or stroma promotes cancer (Marcellini et al., 2006).

We showed that the anti-PlGF monoclonal antibody (mAb) 5D11D4 slows tumor growth in preclinical models, in part by blocking angiogenesis and inflammation (Fischer et al., 2007). However, anti-PlGF mAbs generated by Bais et al. were ineffective in mouse tumor models (Bais et al., 2010), questioning whether the activity of 5D11D4 could be reproduced by independently generated anti-PlGF mAbs. Also, issues were raised about the dose and whether the effects of 5D11D4 were related to off-target activity. Furthermore, Bais et al. argued that insufficient genetic evidence supported a role for PlGF in cancer, overall questioning the therapeutic value of anti-PlGF strategies (Bais et al., 2010). Here, we provide genetic evidence for a disease-candidate role of PlGF and underscore the potential of anti-PlGF therapy in cancer by using complementary genetic and pharmacological tools to eliminate, silence, or inhibit PlGF in spontaneous tumor models. We also characterized via which underlying mechanisms loss/inhibition of PlGF blocked tumorigenesis. To obtain independent confirmation, other groups than those involved in our original study (Fischer et al., 2007) contributed autonomously.

RESULTS

Role of PlGF in Carcinogen-Induced Skin Epithelial Tumor Model

We first explored whether loss of PlGF inhibits growth and angiogenesis in a carcinogen-induced skin epithelial tumor model. PlGF levels were low in healthy skin, acutely upregulated by phorbol 12-myristate 13-acetate (PMA) (pg/mg: 13 ± 1 for control versus 55 ± 6 after PMA; n = 12–6; $p < 0.005$), and chronically elevated in small and large papillomas (pg/mg: 145 ± 49 and 192 ± 18; n = 5; $p < 0.001$). Formation of skin papillomas and associated neovessels was delayed in *PlGF*$^{-/-}$ mice (Figures 1A–1D). The average latency after the first PMA application was 3 weeks longer in *PlGF*$^{-/-}$ mice, and by 20 weeks, 94% of wild-type (WT) mice but only 59% of *PlGF*$^{-/-}$ mice developed tumors (Figures 1E and 1F). *PlGF*$^{-/-}$ mice formed 66% fewer papillomas per mouse. Similar effects were observed for large papillomas (>3 mm). In *PlGF*$^{-/-}$ mice, the first large papilloma developed 4 weeks later than in WT mice (Figures 1G and 1H). At 20 weeks, the incidence of large papillomas was 50% in WT mice but only 29% in *PlGF*$^{-/-}$ mice, and the number of large papillomas per mouse was decreased by 80%. Loss of PlGF impaired the growth of neovessels in healthy skin around the tumors (Figures 1B and 1D). Within papillomas, PlGF deficiency did not affect vessel densities but reduced their size by 65% and 55% in small and large papillomas, respectively (n = 5; $p < 0.05$), whereas the accumulation of macrophages, mast cells, or T cells was not affected (not shown).

Antitumor Activity of the Mouse Anti-Human PlGF mAb 16D3

To extend the genetic evidence for a role of PlGF in cancer, we also sought additional pharmacological evidence for a therapeutic potential of anti-PlGF in cancer and therefore evaluated if the mouse anti-human PlGF mAb 16D3 (dissociation constant [K_D] = 12 pM for human PlGF-1) could reproduce the anticancer activity of 5D11D4; this mAb was generated independently of 5D11D4 by immunizing *PlGF*$^{-/-}$ mice with human PlGF-2. Delivery of 16D3 dose-dependently elevated plasma 16D3 levels (Figure S1A available online). At 12.5 mg/kg, 2×/wk, 16D3 inhibited growth of MDA-MB-435 tumors in immunocompromised mice by 40% (mm^3: 1670 ± 194 for control versus 998 ± 210 for 16D3; n = 12; $p = 0.03$). 16D3 also inhibited the growth of human pancreatic DanG xenografts (Figures S1B–S1D) and cancer-associated cachexia (loss in body weight: 14% in control versus 7% in 16D3; n = 9–10; $p = 0.04$). Both tumors produced human PlGF (pg/mg protein in tumor lysates: 19 ± 5 for MDA-MB-435; n = 12 and 103 ± 37 for DanG; n = 11).

PlGF Blockage Retards Hepatocellular Carcinoma Growth

We then used two hepatocellular carcinoma (HCC) models to characterize more extensively the effects and mechanisms of PlGF blockage. To exclude that germline PlGF deficiency induces compensatory changes that favor tumor inhibition independently, we tested whether conditional PlGF silencing inhibited growth of HCC. In the first model, transgenic expression of an SV40 T-antigen oncogene induced hyperplasia/dysplasia (4–8 weeks), nodular adenoma (12 weeks), and diffuse carcinoma (>16 weeks) (Dupuy et al., 2003). PlGF was undetectable in healthy hepatocytes but apparent in HCC, whereas Flt1 was upregulated in macrophages, Kupffer cells, and vessels (not shown). By RT-PCR, *PlGF* transcripts were upregulated to 295% ± 28% of normal levels in adenomas (n = 4; $p < 0.05$). Hepatic PlGF was silenced by treating HCC mice from 8 to 15 weeks with *PlGF*-specific siRNA, reducing PlGF protein levels by 60% ± 8% (n = 5; $p < 0.05$). Despite incomplete PlGF silencing, hepatomegaly was reduced, with the largest inhibition when PlGF expression and macrophage infiltration were maximal (see below) (Figure 1I); fewer and smaller tumor nodules were present at 15 weeks (superficial nodules 0.5–1 cm and >1.0 cm: 12.7 ± 2.9 and 6.0 ± 0.7 in untreated versus 12.0 ± 1.4 and 4.7 ± 1.1 in control siRNA, and 1.0 ± 0.7 and 0 ± 0 in *PlGF*-specific siRNA, n = 3; $p < 0.005$; Figures 1J–1M).

We also used a carcinogen-induced HCC model by treating mice with diethylnitrosamine (DEN), which causes fibrosis and dysplastic lesions at 16 weeks and hypervascularized tumors by 25 weeks. Hepatic PlGF levels were not acutely upregulated by DEN (not shown) and remained initially low (pg/mg: 2.9 ± 0.7 in healthy versus 1.5 ± 0.4 after 4 weeks DEN; n = 6; p = not significant [NS]) but increased to 423 ± 77 pg/mg in end-stage tumor nodules (n = 6; $p < 0.05$). After 30 weeks of DEN treatment, 58% of WT mice (n = 24) but only 5% of *PlGF*$^{-/-}$ mice (n = 21) succumbed ($p = 0.002$, log rank) and fewer tumor nodules were present in *PlGF*$^{-/-}$ mice (nodules/liver: 17.9 ± 2.2 in WT versus 5.9 ± 2.4 in *PlGF*$^{-/-}$; n = 18; $p = 0.002$). When WT mice with established HCC were treated with 5D11D4 (20 mg/kg;

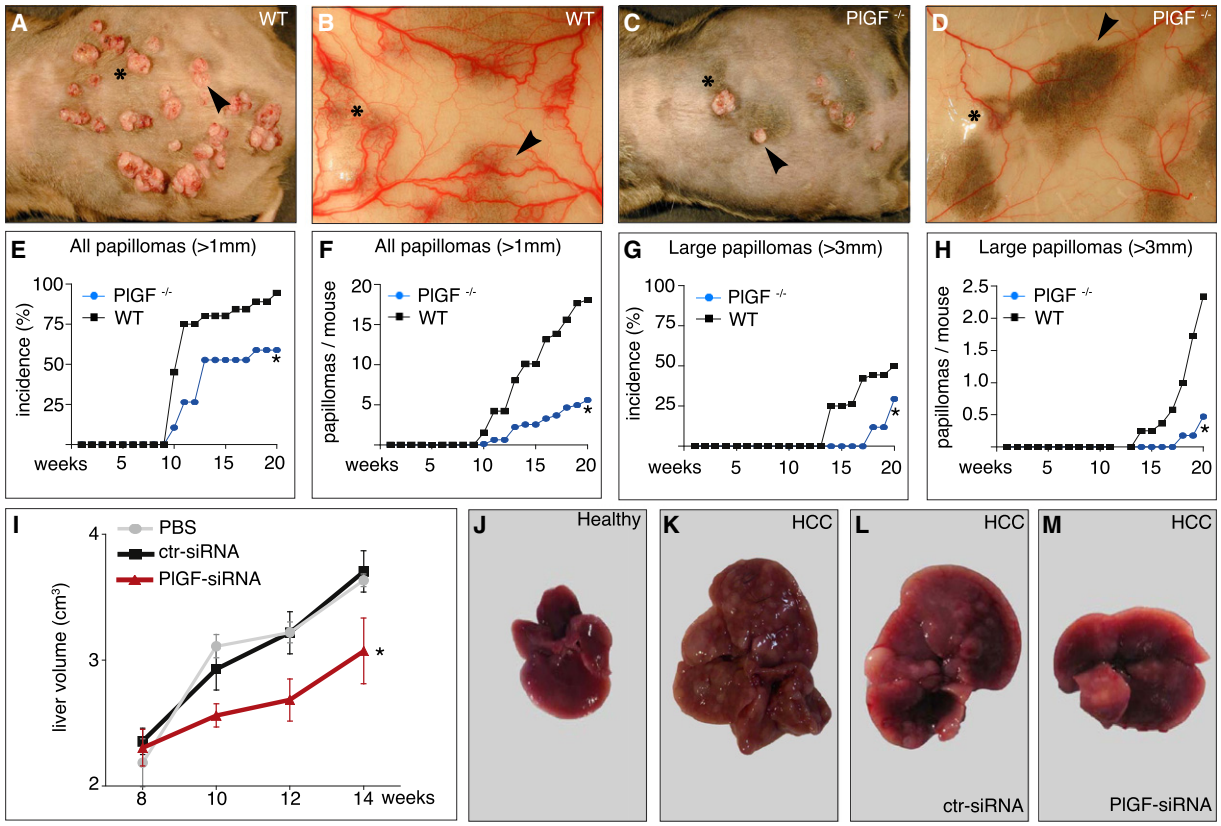

Figure 1. Reduced Papilloma Formation and HCC upon PlGF Blockage

(A–D) Skin papillomas from external (A and C) or internal view (B and D) in *PlGF*$^{-/-}$ (C and D) and WT mouse (A and B). Asterisks and arrowheads indicate corresponding anatomical tumor locations.

(E–H) Incidence (E and G) and number of papillomas per mouse (F and H) (n = 19–20; $p < 0.01$).

(I) Echographic measurement of liver volume in healthy mice and in HCC mice, untreated or treated with *PlGF*-specific or control siRNA (mean ± SEM; n = 6–8; *$p < 0.05$); healthy liver volumes: 0.74 ± 0.05, 0.8 ± 0.1, 0.88 ± 0.06, and 0.72 ± 0.05 cm^3 at 8, 10, 12, and 14 weeks (n = 6).

(J–M) Micrograph of livers from healthy (J) or HCC mice (K–M), untreated (K), control siRNA-treated (L), or PlGF-specific siRNA-treated (M).

See also Figure S1.

2×/wk) from 25 weeks onward for 5 weeks, 45% of mice receiving control IgG died whereas only 23% died in the 5D11D4 group (n = 23–25; $p < 0.05$). Also, 5D11D4-treated mice developed fewer nodules per liver (nodules, all sizes: 21.6 ± 2.9 after control IgG versus 11.1 ± 2.6 after 5D11D4; n = 15; p = 0.02). After 10 weeks of mAb treatment, mortality was 90% in the control group, but it was only 41% after 5D11D4 (n = 11; $p < 0.05$).

PlGF Blockage Inhibits Arterialization and Vessel Abnormalization in HCC

In contrast to the largely portal venous blood supply in healthy livers, the hepatic arterial network expanded substantially in HCC (Figures 2A and 2B), giving rise to the formation of unpaired arteries, i.e., large vessels with a mural coat of smooth muscle actin $(SMA)^+$ cells that are not accompanied by a bile duct (Fernandez et al., 2009). In the transgenic model, PlGF silencing abrogated arterialization, scored arteriographically (Figures 2C–2E) and histologically (lumen size of unpaired arteries: 293 ± 72 μm^2 in ctrl-siRNA versus 70 ± 16 μm^2 in *PlGF*-siRNA; n = 4; $p < 0.05$). In the DEN model, 5D11D4-treated HCC livers contained fewer and smaller unpaired arteries (SMA^+ unpaired vessels: relative area in % of area analyzed and number/mm^2: 5.8 ± 1.0 and 11.3 ± 2.9 after IgG versus 1.4 ± 0.3 and 6.3 ± 0.3 after 5D11D4; n = 7–3; $p < 0.001$ and $p < 0.05$; Figures 2F–2H).

Within HCC nodules, PlGF blockage did not alter capillary density, when counting each branch or profile as a separate vessel (Figures S2A and S2B). However, given that hypoxia stimulates HCC growth (Wu et al., 2007) and that microvascular density does not always provide insight into vessel function (Mazzone et al., 2009), we analyzed other vascular parameters, determining tumor oxygenation. First, we noticed that intercapillary distances were larger and more variable in IgG-treated HCC than in healthy liver (Figures 2I, 2J, and 2O), consistent with reports that rapidly proliferating HCC cells outgrow their vascular supply and thereby become hypoxic (Wu et al., 2007). In fact, large avascular clusters of malignant HCC cells were often found amidst a chaotic capillary network (Figure 2J). In contrast, in PlGF-blocked HCC, intercapillary distances were still variably

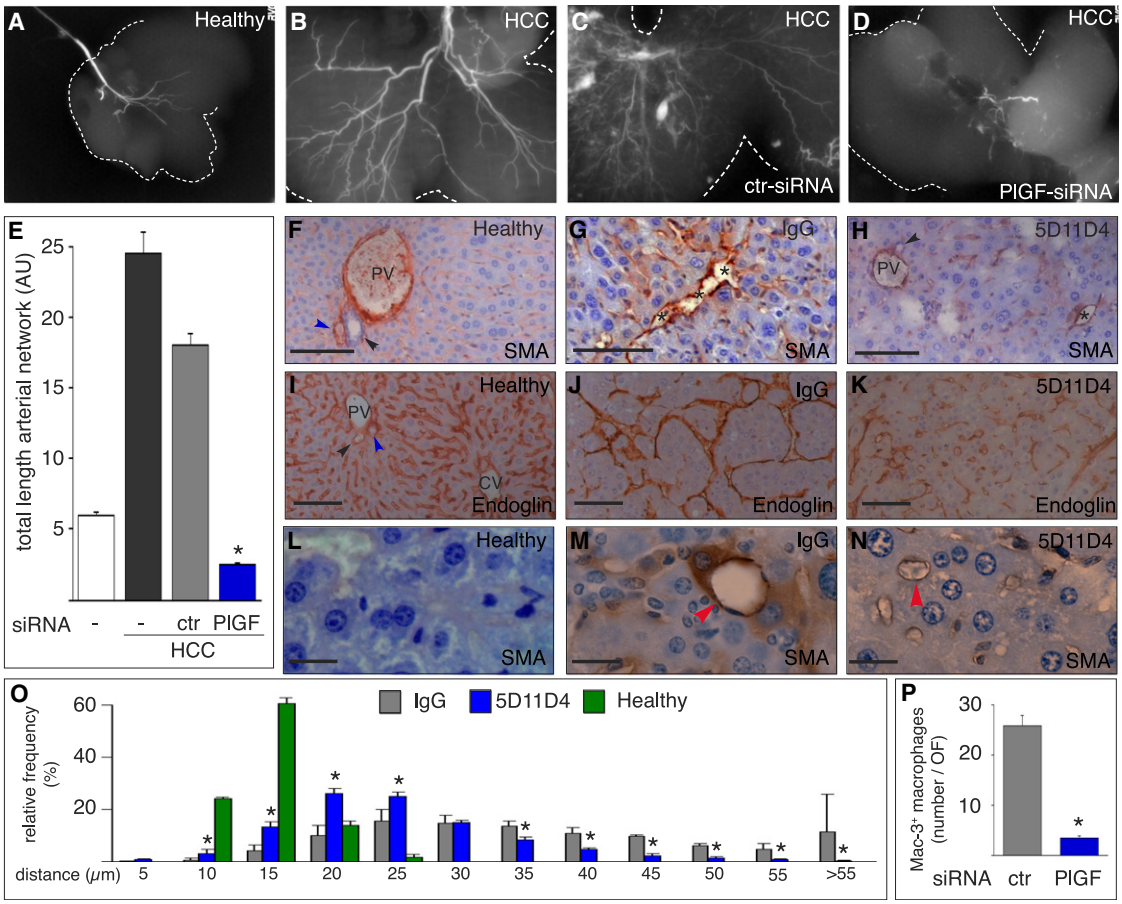

Figure 2. Mechanisms of Anti-HCC Activity by PlGF Blockage

(A–D) Micro-angiography of hepatic arterial supply in healthy (A), untreated HCC (B), control siRNA-treated HCC (C), and *PlGF*-silenced HCC (D) mice.

(E) Quantification of hepatic arterial network in healthy (white bar), untreated HCC (dark gray), control siRNA-treated HCC (light gray), and *PlGF*-silenced HCC (blue) mice (AU: absolute pixel unit, ‰) (n = 4; *p < 0.05).

(F–H) SMA staining, revealing a portal triad with paired hepatic artery in a healthy liver (F), large, smooth muscle cell-coated unpaired arteries (asterisks) in HCC mice treated with IgG (G), and a portal triad and small unpaired artery (asterisk) in HCC liver after 5D11D4 (H). Black arrowhead (bile duct); blue arrowhead (hepatic paired artery); PV (portal vein).

(I–K) Immunostaining for the endothelial marker endoglin, showing portal vein (PV) and central vein (CV) amidst a sinusoidal network in healthy liver (I); black arrowhead (bile duct); blue arrowhead (hepatic paired artery). In IgG-treated HCC nodules, the capillary network is chaotically organized, with tortuous vessels and cords, laying at large distances from each other (J), in contrast to the more regular pattern, size, and shape of capillaries and shorter intercapillary distances in 5D11D4-treated HCC (K).

(L–N) Immunostaining for SMA, showing undetectable expression in HSCs around sinusoids in healthy liver (L). In HCC, tumor capillaries (red arrowhead) are surrounded by strongly SMA^+-stained HSCs in IgG-treated mice (M) but not in 5D11D4-treated mice (N).

(O) Histogram of intercapillary distances, showing shorter distances in 5D11D4-treated HCC; values in healthy liver are shown for comparison.

(P) Mac-3^+ macrophage infiltration in tumors of HCC mice treated with control (gray) or *PlGF*-specific siRNA (blue) (n = 8; *p < 0.05).

Bars: 100 μm (F–K); 20 μm (L–N). Data are mean ± SEM. See also Figure S2 and Table S1.

enlarged but less extensively than in control HCC, thereby creating a more uniform vascular pattern (Figures 2K and 2O).

Second, PlGF blockage counteracted tumor capillary abnormalization, which also determines tumor oxygenation (Mazzone et al., 2009). In HCC nodules, sinusoids lose their characteristics and develop into capillaries (“sinusoidal capillarization”) (Fernandez et al., 2009). Typical for HCC, capillaries become surrounded by activated hepatic stellate cells (HSCs), which express increased levels of SMA, deposit matrix, and release angiogenic and tumorigenic factors (Johnson et al., 1998). These changes increase the resistance to blood flow and impede oxygen delivery, further aggravating hypoxia (Fernandez et al., 2009; Paternostro et al., 2010). A smaller fraction of capillaries was surrounded by SMA^+ HSCs in PlGF-blocked HCC nodules (SMA^+ area around capillaries, %: 5.9 ± 1.3 after IgG versus 2.2 ± 0.6 after 5D11D4; n = 6–7; p = 0.02; Figures 2L–2N).

Furthermore, several capillaries in control HCC nodules had an abnormal shape and size; although approximately half of them had a regular patent lumen, others were present as cords without lumen, and a smaller fraction was very tortuous (Figures 2I and 2J). PlGF blockage partially normalized their abnormal structure. Indeed, in PlGF-blocked tumors, fewer capillaries

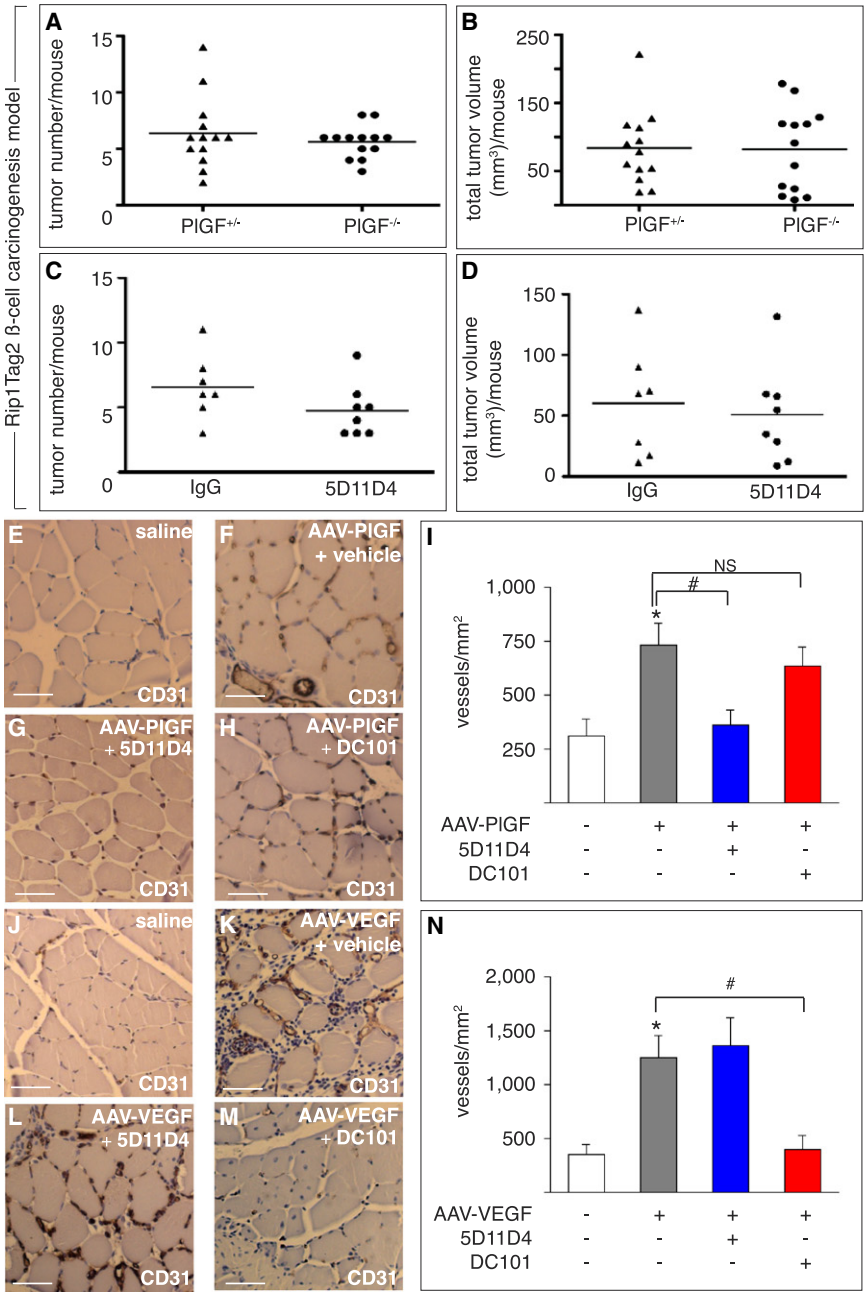

Figure 3. Resistance of Rip1Tag2 Tumors and Evidence for Specificity of 5D11D4

(A–D) The number (A and C) or total volume (B and D) of tumors per mouse were not affected by loss (A and B) or inhibition of PlGF by 5D11D4 (50 mg/kg; 3×/week) (C and D) (n = 7–8); tumor growth in *PlGF*$^{+/-}$*:Rip1Tag2* and *PlGF*$^{+/+}$*:Rip1-Tag2* mice was not different.

(E–I) Intramuscular AAV-PlGF gene transfer-induced angiogenesis (F), which is blocked by 5D11D4 (G) but not by DC101 (H); panel E: control; panel I: quantification of the microvascular density (mean ± SEM; n = 5; *p < 0.05 versus control; #p < 0.05).

(J–N) Intramuscular AAV-VEGF gene transfer-induced angiogenesis (K), which is not affected by 5D11D4 (L) but is reduced by DC101 (M); panel J: control; panel N: quantification of the microvascular density (mean ± SEM; n = 3; *p < 0.05 versus control; #p < 0.05).

Bars: 50 μm. See also Figure S3.

were tortuous or cords and had a more normal appearance (tortuous vessels/mm^2 and cords/mm^2: 44 ± 4 and 237 ± 21 in IgG versus 22 ± 2 and 181 ± 15 in 5D11D4; n = 4–5; p < 0.001 and p = 0.05; Figures 2J and 2K). These changes were functionally relevant, as PlGF-blocked HCC nodules expressed lower levels not only of HIF-2α (HIF-2α$^+$ area, % of nodular area: 28.1 ± 4.3 for IgG versus 14.6 ± 2.6 for 5D11D4; n = 4–5; p < 0.05) but also of other hypoxia-inducible genes (Table S1). Moreover, in line with reports that hypoxia promotes HCC growth, proliferation of HCC cells was higher in avascular clusters (IgG) than in vascular regions with short intercapillary distances (5D11D4) (PCNA$^+$ cells/mm^2: 90 ± 18 after IgG versus 36 ± 2 after 5D11D4; n = 4; p = 0.02). Additional analysis showed that activated HSCs are a source of proangiogenic PlGF, and that PlGF is a mitogen and chemoattractant for these cells but not for hepatoma cell lines (not shown). Finally, PlGF blockage reduced hepatic macrophage numbers in the transgenic (Figure 2P) and carcinogen model (not shown).

PlGF Blockage or Deficiency Does Not Inhibit Rip1Tag2 Growth

We intercrossed the transgenic Rip1Tag2 model of pancreatic β cell carcinogenesis with *PlGF*$^{-/-}$ mice. No genotypic differences were observed between *Rip1Tag2* × *PlGF*$^{+/-}$ and *Rip1Tag2* × *PlGF*$^{-/-}$ mice in tumor incidence or burden (Figures 3A and 3B) or staging (Figure S3A), despite detectable PlGF expression in WT tumors (Figure S3B). As this tumor growth is independent of PlGF, we used it to test whether 5D11D4 inhibits tumorigenesis via off-target activities. Therefore, 9-week-old transgenics bearing angiogenic tumors were treated with 5D11D4 (50 mg/kg; 3×/week) for 3 weeks until end-stage. Treatment with 5D11D4 failed to affect tumor growth or incidence in Rip1Tag2 mice (Figures 3C and 3D), consistent with the absence of non-PlGF effects on tumorigenesis. That 5D11D4 blocks PlGF specifically without off-target effects was confirmed in additional experiments. Indeed, angiogenesis induced by *PlGF* gene transfer in *PlGF*$^{-/-}$ mice was selectively blocked by 5D11D4 but not by the anti-Flk1/VEGFR-2 mAb DC101 (Figures 3E–3I), whereas DC101 but not 5D11D4 abrogated angiogenesis induced by *VEGF* gene transfer (Figures 3J–3N).

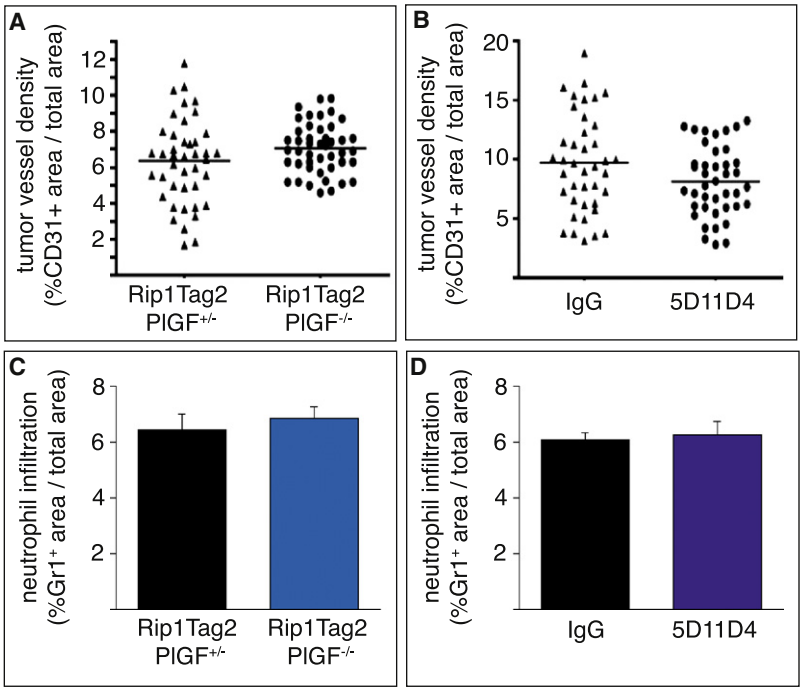

Figure 4. Mechanisms of PlGF Blockage in Rip1Tag2 Tumors

(A and B) Quantification of intratumoral vessel density of tumors from *Rip1Tag2:PlGF*$^{+/-}$ and *Rip1Tag2:PlGF*$^{-/-}$ mice (n = 7) (A) and of tumors from *Rip1Tag2* mice, treated with control IgG or 5D11D4 (n = 7) (B).

(C and D) Quantification of neutrophil infiltration in tumors from *Rip1Tag2:PlGF*$^{+/-}$ and *Rip1Tag2:PlGF*$^{-/-}$ mice (n = 7) (C) and in tumors from *Rip1Tag2* mice, treated with control IgG or 5D11D4 (n = 7) (D). Data are mean ± SEM (C and D).

We also analyzed why Rip1Tag2 tumors were resistant to PlGF blockage. Notably, tumor angiogenesis was not affected by loss or inhibition of PlGF (Figures 4A and 4B). In line with findings that neutrophils mediate the tumor angiogenic switch in this model (Nozawa et al., 2006), infiltration of myeloid cells (primarily neutrophils) was not affected by PlGF blockage (Figures 4C and 4D), likely explaining the refractoriness of this model to PlGF blockage.

5D11D4 Inhibits Choroidal Neovascularization by Blocking PlGF

Bais et al. questioned the specificity of 5D11D4 in targeting PlGF and criticized the use of a single anti-PlGF mAb clone (Bais et al., 2010). To address these questions, we also used a model of choroid neovascularization (CNV). Three days after laser injury, choroidal PlGF levels were upregulated (pg/mg: 168 ± 12 in non-injured versus 343 ± 18 in lasered choroids; n = 3; $p < 0.05$), whereas Flt1 was detected in neovessels and stromal cells (Figure S4A). 5D11D4 accumulated in CNV lesions upon intraperitoneal injection (Figure S4B). Quantification of CNV upon perfusion with FITC-conjugated dextran 14 days after lasering showed that 5D11D4 dose-dependently inhibited CNV, with a maximal effect at 25 mg/kg, 3×/week (Figures 5A–5C). A comparable inhibition of 60% ± 6% was obtained with 25 mg/kg, 2×/week (n = 10; p = NS versus 3×/week), while intravitreal injection was also effective (not shown). 5D11D4 also inhibited CNV by 53% ± 10% (n = 3; $p < 0.05$) in *Ccl2*$^{-/-}$ mice, a model of age-related macular degeneration (AMD) that better resembles the human condition.

Bais et al. questioned the specificity of 5D11D4 and suggested that Fc-dependent effects might explain its activity (Bais et al., 2010). We reasoned that if 5D11D4 would specifically block PlGF, it should not inhibit CNV beyond the level induced by deficiency of PlGF or its signaling receptor Flt1. Loss of PlGF inhibited CNV, but additional 5D11D4 treatment did not further reduce CNV lesions (Figure 5D). Likewise, CNV was inhibited in *Flt1-TK*$^{-/-}$ mice (indicating that Flt1 signaling is critical and Flt1 does not act as a VEGF-trap alone), but 5D11D4 did not further reduce CNV lesions in these mice (Figure 5E).

To assess whether the Fc-fragment of 5D11D4 was required, we generated 5D11D4/Fab fragments (K_D = 1.51 nM). At 100- to 400-fold molar excess, Fab inhibited the binding of PlGF to Flt1 (IC_{50} = ~1.1 nM), neutralized Flt1 tyrosine phosphorylation in response to PlGF (response above control: 217% for PlGF; 0% for PlGF + 5D11D4/Fab; 15% for PlGF + 5D11D4), and blocked the chemotactic activity of PlGF for macrophages (migrated cells/optical field: 169 ± 42 for control; 11 ± 17 for 5D11D4; 0 for 5D11D4/Fab; n = 6; $p < 0.05$). Compared to control IgG/Fab, intra-ocular injection of 5D11D4/Fab inhibited CNV formation at 5 days by 41% (neovascular area, ×103 μm^2: 16.6 ± 2.0 after IgG/Fab versus 9.8 ± 1.7; n = 51–43; p = 0.01). Similar data were obtained with recombinant 5D11D4/Fab (K_D = 0.57 nM) (not shown).

Other anti-mouse PlGF mAb clones were used to reproduce the 5D11D4 data. Of two other mAbs that bound to PlGF with high affinity and blocked binding of PlGF to Flt1 in vitro, 3C7A8 (K_D = 3.4 nM) inhibited CNV, whereas 12H6B5 (K_D = 4.3 nM) only showed a tendency (Figure 5F), even despite the fact that plasma levels were >100 μg/ml for all mAbs. Thus, certain anti-PlGF mAb clones with proven blockage of PlGF binding to its receptor in vitro may still not be able to block PlGF-driven processes in vivo.

As an independent confirmation of 5D11D4's specificity, we tested whether 16D3 blocked human PlGF-driven CNV in vivo. Whereas delivery of human PlGF-2 via osmotic minipump (10 μg/week) increased CNV lesions in humanized *PlGF*$^{-/-}$ mice, treatment with 16D3 (25 mg/kg; 3×/week) reduced CNV to levels similar to those in *PlGF*$^{-/-}$ mice (Figure 5G). Similar data were obtained when *PlGF*$^{-/-}$ mice were humanized by intravenous injection of the adenoviral vector Ad.hPlGF2, which elevated circulating human PlGF-2 plasma levels to 200–300 ng/ml. By day 14, Ad.hPlGF2 increased CNV formation nearly to levels in WT mice, yet delivery of 16D3 (25 mg/kg, 2×/week, resulting in plasma 16D3 titers of 100–300 μg/ml) completely inhibited CNV formation (Figure S4C).

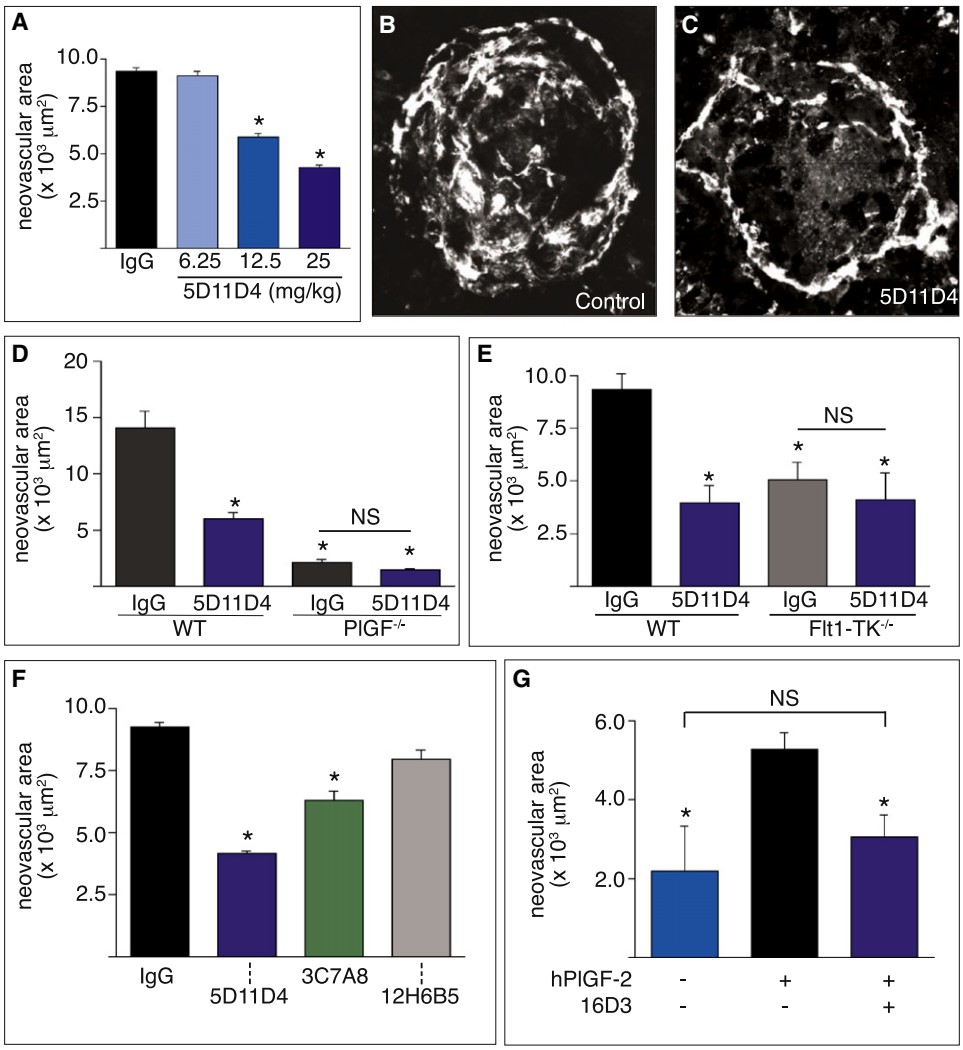

Figure 5. Inhibition of CNV by Anti-PlGF or PlGF Deficiency

In all panels, analysis was 14 days after lasering; mAb (3×/week) was started 3 hr after lasering until sacrifice.

(A) Dose-dependent inhibition of CNV by 5D11D4 (n = 12/group; *p < 0.05).

(B and C) FITC-dextran flatmounts, revealing fewer choroidal neovessels after 5D11D4 (C) than control IgG (B).

(D) CNV was reduced in *PlGF*$^{-/-}$ mice, but 5D11D4 treatment (25 mg/kg) did not further reduce CNV in *PlGF*$^{-/-}$ mice (n = 10/group; *p < 0.05 versus WT, control IgG).

(E) Flt-TK deficiency reduced CNV but 5D11D4 (25 mg/kg) did not further reduce CNV (n = 6/group; *p < 0.05 versus WT, IgG).

(F) Inhibition of CNV by anti-PlGF mAb 3C7A8, whereas 12H6B6 only exhibited a tendency (25 mg/kg) (n = 6/group; *p < 0.05).

(G) Delivery of human PlGF-2 (10 µg/week) stimulated CNV in *PlGF*$^{-/-}$ mice; hPlGF-driven CNV was blocked by 16D3 (25 mg/kg) (n = 5/group; *p < 0.05 versus hPlGF-2 without 16D3).

Data are mean ± SEM. See also Figure S4.

5D11D4 Enhances VEGF-Targeted Inhibitors

Bais et al. questioned whether anti-PlGF mAbs enhanced VEGF-inhibitor treatment (Bais et al., 2010). We thus evaluated whether 5D11D4 enhanced the effect of VEGF inhibitors by testing the anti-Flk1 mAb DC101. At a dose of 6.25 to 50 mg/kg (3×/week), DC101 inhibited CNV (Figures 6A–6C). In line with tumor studies (Fischer et al., 2007), DC101 elevated plasma PlGF levels 3 days after laser injury (pg/ml: 11 ± 1.1 after IgG versus 330 ± 49 after DC101; n = 5; p < 0.05). Because of the role of PlGF in CNV and its upregulation by DC101, we explored whether 5D11D4 could partially substitute DC101 without compromising DC101's maximal effect. Compared to monotherapy with a low dose of 12.5 mg/kg DC101 or 25 mg/kg 5D11D4, the combination of 5D11D4 plus DC101 reduced CNV formation more extensively, i.e., comparably to the maximal dose of DC101 monotherapy (Figure 6D). These substitution results in the CNV model mimic those in previous cancer studies (Fischer et al., 2007).

Additionally, we used hydroporation gene transfer to elevate plasma levels of soluble Flk1 (sFlk1, which traps VEGF) to

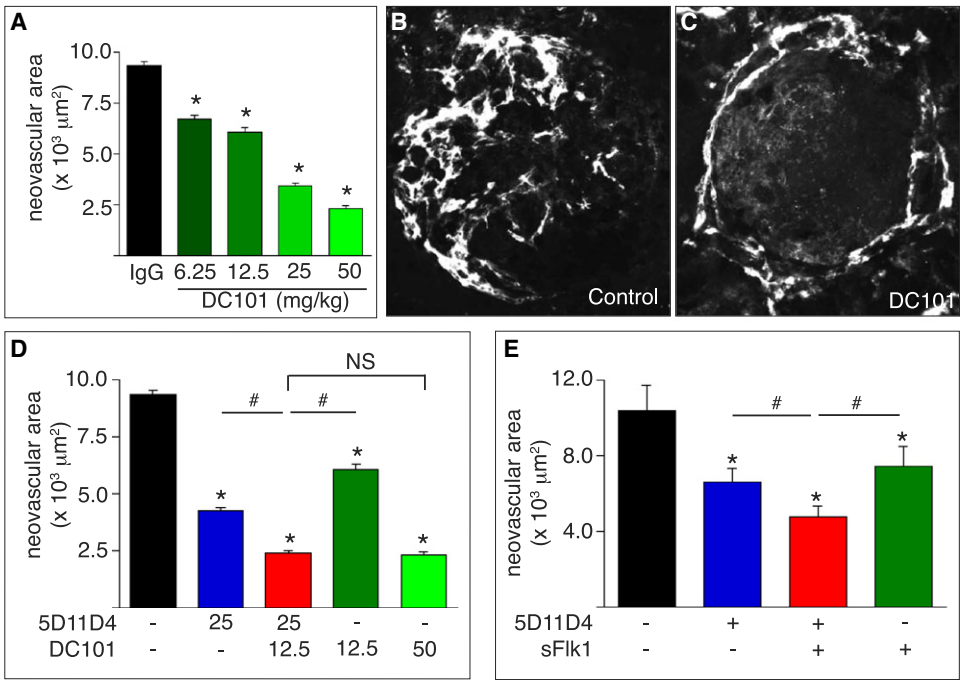

Figure 6. 5D11D4 Enhances Inhibition of CNV by VEGF Inhibitors

In all panels, analysis was 14 days after lasering; mAb (3×/week) was started 3 hr after lasering until sacrifice.

(A) Dose-dependent inhibition of CNV by DC101 (n = 12/group; *p < 0.05).

(B and C) FITC-dextran choroidal flatmounts, revealing fewer perfused neovessels after DC101 (C) than control IgG (B).

(D) Partial replacement of DC101 with 5D11D4 yielded similar anti-CNV effect as maximal DC101 dose alone (n = 12/group; *p < 0.05 versus control; #p < 0.05 versus monotherapy); dose (mg/kg) of 5D11D4 and DC101 is indicated below each bar.

(E) Combination of 5D11D4 (25 mg/kg) plus gene transfer of sFlk1 (hydroporation 2 days before lasering) inhibited CNV more than either monotherapy (n = 8–11; *p < 0.05 versus control; #p < 0.05 versus monotherapy).

Data are mean ± SEM.

5.2 ± 1.5 µg/ml by day 5 (Davidoff et al., 2002). Compared to the prominent anti-CNV effect of DC101, sFlk1 reduced CNV only partially (Figure 6E). However, this intermediate inhibition allowed us to explore whether 5D11D4 amplified the anti-CNV effect of sFlk1. Indeed, CNV was inhibited more extensively by the combination of 5D11D4 plus sFlk1 than by either monotherapy (Figure 6E). Thus, as observed in tumors (Fischer et al., 2007), 5D11D4 enhanced the effect of a VEGF-trap.

5D11D4 Inhibits Ocular Angiogenesis and Inflammation

Bais et al. also criticized the ability of anti-PlGF mAbs to block angiogenesis and inflammation (Bais et al., 2010). We thus analyzed whether 5D11D4 and PlGF deficiency inhibited CNV via similar mechanisms, as this would strengthen the conclusion that the mAb acts via specific inhibition of PlGF and not via off-target mechanisms. Since FITC-dextran only labels perfused vessels, we analyzed all neovessels by staining choroidal cross-sections for the endothelial marker CD31. At 25 mg/kg, 5D11D4 reduced total vessel area and vessel density comparably as in *PlGF*$^{-/-}$ mice (Figures 7A and 7B), indicating that 5D11D4 phenocopied the angiostatic *PlGF*$^{-/-}$ mechanisms, not only qualitatively but even (nearly) quantitatively. DC101 similarly inhibited vessel area and density (Figures 7A and 7B).

To characterize the vascular phenotype further, we used scanning electron microscopy (SEM) to visualize microvascular corrosion casts. In WT mice, a dense network of choroidal neovessels sprouted from the adjacent healthy tissue into the lesion (Figures 7C and 7D). By contrast, in 5D11D4-treated WT and in *PlGF*$^{-/-}$ mice, fewer neovessels sprouted and branches only formed short aborted stumps (Figures 7E–7H). DC101 induced a distinct defect, characterized by fewer sprouts with only a few side branches and spiky projections, and the endothelium appeared almost frozen (Figures 7I and 7J). Loss or inhibition of PlGF also comparably blocked choroidal vessel leakage (Figures S5A and S5B; not shown). Macrophage infiltration was also inhibited by PlGF blockage. In WT mice, 5D11D4 reduced the F4/80^{+} area, whereas DC101 had no effect (Figures 7K–7M); this may explain why DC101 reduced lesion thickness less extensively than 5D11D4 (not shown). The F4/80^{+} area was comparably reduced in *PlGF*$^{-/-}$ mice (Figure 7K).

DISCUSSION

Bais et al. questioned the disease role of PlGF and therapeutic potential of anti-PlGF mAbs (Bais et al., 2010). First, they indicated that there is insufficient genetic evidence for a role of PlGF in cancer. We show that PlGF deficiency delays

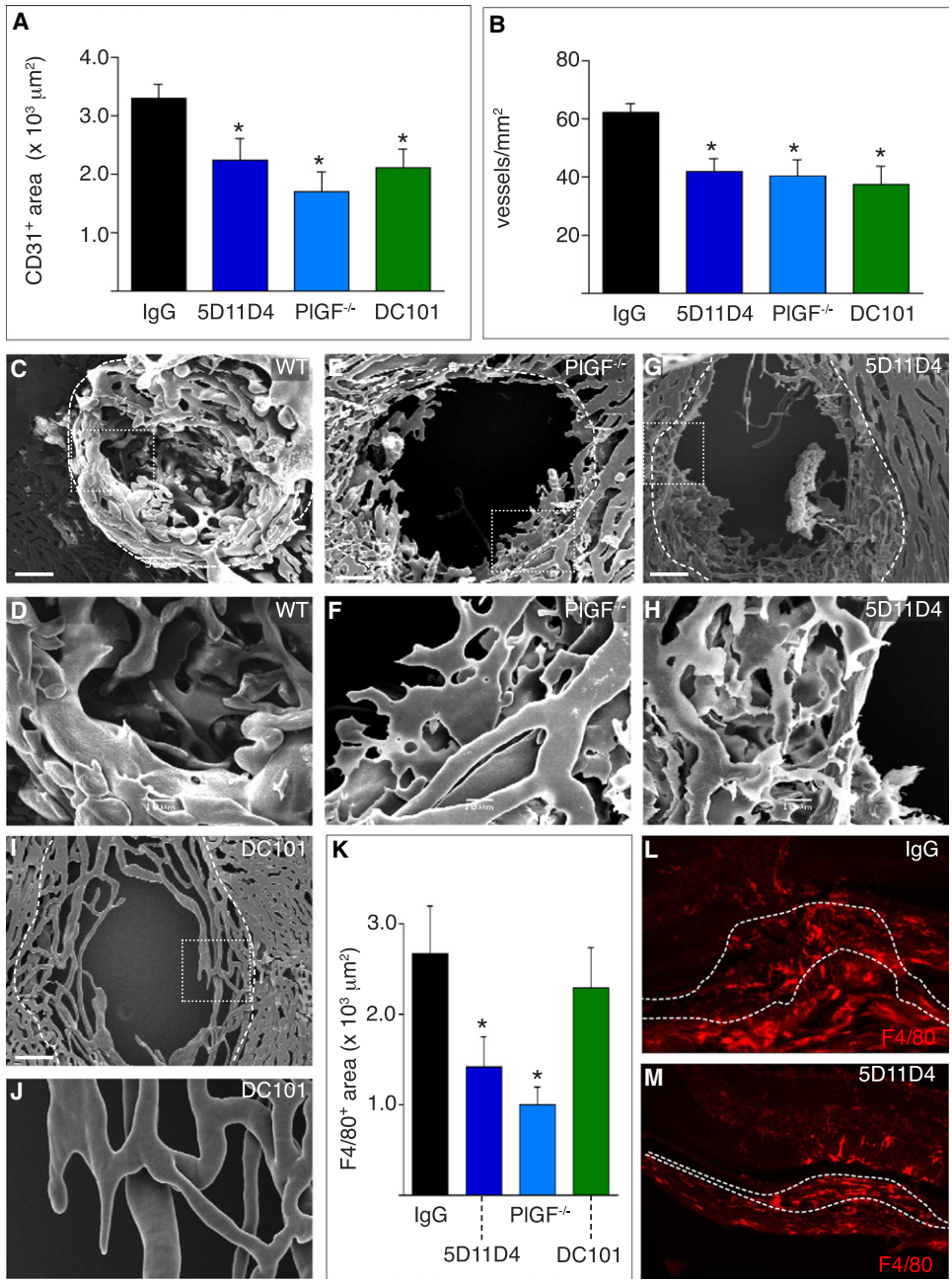

Figure 7. Mechanisms of CNV Inhibition by PlGF Blockage

Analysis at days 14 (A–J) or 5 (K–M) after lasering; mAb treatment (3×/week) started 3 hr after lasering until sacrifice.

(A and B) PlGF deficiency and 5D11D4 (25 mg/kg) reduced $CD31^+$ area (A) and vessel density (B) (n = 10; *p < 0.05 versus control). The antiangiogenic effect of DC101 (25 mg/kg) is shown for comparison.

(C–J) SEM micrographs of CNV in WT (C and D), *PlGF*$^{-/-}$ (E and F), 5D11D4-treated WT (G and H), and DC101-treated WT (I and J) mice. Dashed line: border between laser-induced necrotic center (black hole) and adjacent healthy choroid, from where neovessels sprout. In WT mice, vessels of irregular size and shape sprouted into the wound. By contrast, in *PlGF*$^{-/-}$ and 5D11D4-treated WT mice, neovessels only formed aborted stumps, despite numerous spiky protrusions. After DC101, neovessels appeared immobilized ("frozen") and exhibited signs of pruning with few sprouts. Bars: 50 µm (C, E, G, and I); 10 µm (D, F, H, and J).

(K) Absence of PlGF or 5D11D4 (25 mg/kg) inhibits accumulation of $F4/80^+$ macrophages in CNV, whereas DC101 is ineffective (n = 10/group; *p < 0.05).

(L and M) F4/80 immunostaining of CNV lesions, showing reduced macrophage infiltration after 5D11D4 (25 mg/kg) (L) as compared to IgG (M). Dashed lines: borders of CNV lesion.

Data are mean ± SEM. See also Figure S5.

carcinogen-induced HCC and papilloma formation, and that PlGF silencing retards transgenic HCC, consistent with reports that PlGF levels correlate with a poor outcome in HCC patients (Ho et al., 2006). Moreover, silencing of tumor cell-derived PlGF causes regression of pediatric brain tumors (R. Jain, personal communication). Though our study provides initial loss-of-function genetic evidence for a role of PlGF in spontaneous cancer models, caution is warranted to generalize the role of PlGF in cancer, as Rip1Tag2 tumors are resistant.

A second concern was whether the 5D11D4 effects are specific. Independent evidence argues that 5D11D4's activity is specific. First, the anticancer and anti-CNV effects by 5D11D4 and 16D3 are phenocopied by the loss of PlGF or Flt1 in the models studied. Similar findings were obtained independently in pediatric brain tumors (R. Jain, personal communication). Even the lack of an effect of PlGF deficiency and 5D11D4 treatment on Rip1Tag2 tumors suggests that 5D11D4 does not induce off-target effects. Furthermore, the safety profile of 5D11D4 in mice (Fischer et al., 2007) and of the humanized anti-human PlGF mAb TB403 in humans (Lassen et al., 2009; Riisbro et al., 2009) resembles the lack of disease development in *PlGF*$^{-/-}$ mice (Carmeliet et al., 2001). Overall, when *PlGF*$^{-/-}$ and 5D11D4 effects were compared, 5D11D4 mimicked each *PlGF*$^{-/-}$ phenotype analyzed so far (Table S2), supporting a specific activity of 5D11D4.

Another argument for the specificity of 5D11D4 is that delivery of this mAb and loss of PlGF induced similar mechanisms, albeit with contextual differences. For instance, angiogenesis was inhibited comparably by loss or inhibition of PlGF in CNV. In HCC, silencing or inhibition of PlGF reduced arterialization and tumor vessel abnormalization. Angiogenic defects were also observed in papillomas, reminiscent of those seen after PlGF loss or inhibition in implanted tumors and other diseases (Carmeliet et al., 2001; Fischer et al., 2007) as well as in ischemic retina in an independently generated *PlGF*$^{-/-}$ model (E. Cheung et al., IOVS 2009;50:ARVO E-Abstract 2943). Arterialization defects in PlGF-blocked HCC resemble those in portal hypertension and limb revascularization in *PlGF*$^{-/-}$ mice (Carmeliet et al., 2001; Van Steenkiste et al., 2009). Also, in CNV and HCC, loss, silencing, or inhibition of PlGF impaired macrophage accumulation, as in skin inflammation and atherosclerosis (Oura et al., 2003; Roncal et al., 2010). In papilloma, PlGF deficiency did not prevent macrophage accumulation, but because myeloid cells promote release of proangiogenic PlGF, blockage of macrophage-derived PlGF can contribute to impairing papilloma growth. Moreover, effects of PlGF blockage on macrophage polarization should not be excluded (C. Rolny, personal communication). Our findings that PlGF blockage does not necessarily need to affect microvascular density or macrophage counts in order to inhibit growth of certain tumors highlight the context-dependent multitasking activity of PlGF and the need to analyze vessel size or function as well. Obviously, in other situations, for instance when 5D11D4 treatment of a chronic disease is initiated at advanced stages, short-term PlGF inhibition may induce different mechanisms than permanent *PlGF* gene inactivation.

A third concern was that only a single anti-PlGF mAb clone was used. Chemical PlGF blockage inhibits growth and metastasis of xenografts (Taylor and Goldenberg, 2007) and anti-PlGF antiserum blocks PlGF-induced leakage (Carmeliet et al., 2001). Here, the anticancer/anti-CNV activity of 5D11D4 was reproduced by independently generated anti-mouse (3C7A8) and anti-human (16D3) PlGF mAbs. Similar to the Bais study (Bais et al., 2010), we also obtained mAb clones that recognized PlGF and blocked its binding to Flt1 in vitro but lacked efficacy in vivo. The precise reasons heretofore remain to be defined, but an outstanding question is whether immunization of *PlGF*$^{-/-}$ mice with "foreign" PlGF might have yielded mAbs with distinct properties for inhibiting PlGF in situ. Whether differences in physicochemical properties, posttranslational modifications, or other alterations may influence their efficacy also remains to be determined. An increased affinity and potency of anti-VEGF mAbs in vitro did also not directly correlate with antiangiogenic potency or efficacy in vivo (Gerber et al., 2007).

It is also relevant to note that we identified a spontaneous tumor model that was refractory to PlGF loss or inhibition, indicating that PlGF is not a disease-promoting factor in all tumors and that other tumor models could be refractory to anti-PlGF as well. The resistance of the Rip1Tag2 model to PlGF blockage is likely due in part to the inability of PlGF loss or inhibition to block the infiltration of neutrophils, key mediators of the angiogenic switch in this model (Nozawa et al., 2006). As other tumors can be resistant, it will be relevant to study the underlying mechanisms and identify predictive biomarkers.

Fourth, the dose of 5D11D4 was criticized. Initially, we used 50 mg/kg, even though signs of efficacy were noticed at 12.5 mg/kg (Fischer et al., 2007). This is higher than the dose used for other mAbs against (un)related targets (1 to 10 mg/kg) but comparable to the dose used for DC101 or anti-Flt1 (40 mg/kg). Anti-VEGF mAbs are used clinically at 5 to 15 mg/kg. In more recent studies, we obtained anti-disease activity in atherosclerosis, CNV, and HCC with 5D11D4 at 20–25 mg/kg, delivered only two times per week (Roncal et al., 2010). Furthermore, 16D3 inhibited human cancer xenografts at 12.5 mg/kg, and statistically significant tumor growth inhibition has been observed with the humanized anti-human PlGF mAb TB403 in a human RCC xenograft at doses as low as 3 mg/kg (C. Rizzo, personal communication). Disease stabilization for 12 months has been observed with TB403 at 5 mg/kg in 2 out of 23 cancer patients with advanced disease refractory to standard therapy (Lassen et al., 2009; Riisbro et al., 2009).

Related to Bais' remark that 5D11D4 is in vast excess of its ligand (Bais et al., 2010), it is noteworthy that anti-VEGF also circulates in vast excess over its ligand. Indeed, in cancer patients and mice, comparable plasma levels were reported for VEGF and PlGF (10 to 100 pg/ml) and for anti-VEGF and anti-PlGF mAbs delivered at effective doses (300 to 600 μg/ml), resulting in >10^6-fold excess of mAb over ligand (Gordon et al., 2001; Lassen et al., 2009; Riisbro et al., 2009). Furthermore, it should be noticed that in the gene transfer experiments, 16D3 blocked CNV, even though its plasma titers were only 10^3-fold higher than circulating human PlGF levels.

Although we do not question the findings of Bais et al. (Bais et al., 2010), we also do not have a unifying explanation, and additional studies will be required to resolve the Matters Arising. For instance, an outstanding question is how our *PlGF*$^{-/-}$ data can be reconciled with *Flt1-TK*$^{-/-}$ data. Controversial findings

on tumor growth in *Flt1-TK*$^{-/-}$ mice will need to be resolved as well (Dawson et al., 2009; Hiratsuka et al., 2002), and the fact that *Flt1-TK*$^{-/-}$ mice upregulate VEGF highlights the complexity of this model (Wittko et al., 2009), cautioning against oversimplified interpretations of data in this model.

Even though HCC is a "hypervascular" cancer, it is characterized by hypoxia, and its growth is promoted by hypoxia (Wu et al., 2007). Paradoxically, even though hypoxic HCC cells try to improve their oxygenation by stimulating the arterial blood supply, they impair oxygen delivery by inducing capillary "vessel abnormalization" in tumor nodules. Moreover, because of their aggressive nature, they outgrow their vascular supply, thereby enlarging intercapillary distances and aggravating hypoxia. This initiates a self-reinforcing vicious cycle of nonproductive HCC vascularization, which *impairs* instead of *improves* tumor oxygenation and promotes malignancy. By inducing vessel normalization, PlGF blockage interrupts this cycle, creates a less oxygen-deprived and oncogenic microenvironment, and reduces the need for arterialization. Given that VEGF inhibitors may fuel metastasis by evoking hypoxia (Loges et al., 2009), the anti-abnormalization activity of anti-PlGF may offer a novel mechanistic framework to combat HCC.

Anti-VEGF therapy offers improvement of vision in patients with AMD but requires *intravitreal* injection with a risk of adverse effects. The safety profile of anti-PlGF warrants further study if *systemic* delivery of anti-PlGF mAbs can be used to partially replace anti-VEGF in at-risk patients. Finally, results of phase I clinical trials show that TB403 was well tolerated without increased risk of adverse effects in healthy volunteers and terminal cancer patients but with initial signs of disease stabilization in 6 of 23 cancer patients (Lassen et al., 2009; Riisbro et al., 2009). Future clinical studies will be required to assess the therapeutic potential of anti-PlGF strategies in cancer and non-oncology indications, but, by their very nature, such developments represent complex challenges.

EXPERIMENTAL PROCEDURES

Additional information is available in the Extended Experimental Procedures.

Animals

C57BL/6, Swiss, and nude mice were from Charles River, Belgium; Balb/C mice from Harlan, Netherlands; *Ccl2*$^{-/-}$ mice from Jackson Laboratory. *PlGF*$^{-/-}$ mice were described (Carmeliet et al., 2001). *Flt1-TK*$^{-/-}$ mice were provided by M. Shibuya. Animal procedures were approved by ethical committees.

Monoclonal Antibodies

mAbs against murine or human PlGF-2 were generated in *PlGF*$^{-/-}$ mice. Fabs were obtained by papain digestion; recombinant Fabs were generated by coexpression of the heavy chain and light chain variable domain in *E. coli* (see Extended Experimental Procedures). Kinetic analysis of antibody/ligand was performed using surface plasmon resonance. mAb biotinylation was performed using EZ-link Sulfo-NHS-LC-Biotin.

Tumor Mouse Models

Evaluation of tumor incidence and growth, immunostaining, and morphometry of vascular, inflammatory, and other parameters are specified in the Extended Experimental Procedures.

Skin Carcinogenesis Model

For tumor initiation, 25 μg 7,12-dimethylbenz[a]anthracene (Sigma) was applied topically to shaved skin of 8-week-old female mice (129/Sv), followed by weekly topical application of 5 μg PMA for 20 weeks (Hawighorst et al., 2001). Lesions with a diameter >1 mm present for > 1 week were recorded as a tumor.

Trangenic HCC Model

Male C57Bl6/ASV-B mice, expressing SV40 T-Ag in hepatocytes, developed HCC (Dupuy et al., 2003). Control and *PlGF* siRNA (Dharmacon Custom siSTABLE SMART pool; Perbio Sciences) were injected intraperitoneally (i.p.) every 3 days from weeks 8 to 15 (2.5 μg/g).

DEN-Induced HCC Model

Five-week-old male WT and *PlGF*$^{-/-}$ mice (129/Sv) received weekly i.p. injections with DEN (35 mg/kg). Wild-type mice were treated with 5D11D4 or IgG (20 mg/kg; 2×/week).

Rip1Tag2 Mouse Model

Rip1Tag2 mice were crossed with *PlGF*$^{-/-}$ mice (C57Bl/6) or treated with 50 mg/kg 5D11D4 or IgG for 3 weeks from 9 weeks. Tumor analysis of *Rip1Tag2:PlGF*$^{-/-}$ and *Rip1Tag2:PlGF*$^{+/-}$ littermates was performed at 12 and 13 weeks.

Tumor Xenografts

10^7 MDA-MB-435 cells were injected subcutaneously (s.c.) in 8-week-old triple immunodeficient Beige Nude XIC NIHIII mice; 10^7 human pancreatic DanG tumor cells were s.c. injected in 11-week-old female *nu/nu* mice. Mice were randomized for treatment at 60 mm^3 tumor volume. 16D3 or control IgG were injected i.p. All analyses were as described (Fischer et al., 2007). 16D3 levels were measured by anti-mouse IgG ELISA using hPlGF-1-coated plates.

Choroidal Neovascularization Model

CNV was induced in C57BL/6 mice by laser burn. Mice were injected i.p. with 5D11D4, DC101, or control IgG, 2–3×/week until days 5 or 14, or intravitreally with 5D11D4/Fab or control IgG/Fab on days 0 and 3. CNV was measured by investigators masked to treatment and confirmed independently by investigators in three laboratories (VRC, UIG, and TG). For sFlk1 gene transfer, 40 μg of a vector encoding sFlk1 or control was injected intravenously (i.v.). Plasma sFlk1 was determined by immunoassay (R&D Systems). Groups involved ten mice (unless otherwise stated) and experiments were repeated 3×. Histology and immunostaining were as described (Carmeliet et al., 1998; Fischer et al., 2007; Luttun et al., 2002b). Eyes were enucleated after intracardial or retrobulbar perfusion with FITC-conjugated dextran, flat mounted (left eye), or processed for immunohistology (right eye). The CNV area, total lesion area, and their ratio were analyzed using a Zeiss Axio Imager Z1 microscope with macros (KS300 image analysis software) on FITC-perfused flat mounts. Immunostainings for CD31, F4/80, PlGF, and Flt1, morphometric analysis of neovascular area, vessel density, and inflammation, and SEM on choroidal corrosion casts were performed as in the Extended Experimental Procedures. PlGF levels in choroids were determined by ELISA (R&D Systems). To humanize *PlGF*$^{-/-}$ mice, human PlGF-2 protein or gene was administered via osmotic minipumps (10 mg/week for 14 days) or adenoviral injection (3 × 109 pfu in 100 μl, i.v.); on day 2, eyes were lasered and mice were injected i.p. every 2 days with 16D3 (25 mg/kg) or control IgG. Macrophage migration, Flt1 phosphorylation, and limb muscle angiogenesis were performed as in the Extended Experimental Procedures.

Statistics

All data are mean ± standard error of the mean (SEM). Statistical significance was calculated by two-sided unpaired or paired (for body weight loss data) Student's t test (Prism). Tumor growth curves (tumor xenografts) were analyzed using a general linear model (Univariate ANOVA), with correction for the experiment (two independent experiments) or by two-way ANOVA (SPSS). HCC mortality scores were analyzed by log rank test, and vessel distance distribution scores by Chi-square. In the legends, the number of mice refers to the size of the group shown in the representative experiment.

SUPPLEMENTAL INFORMATION

Supplemental Information includes Extended Experimental Procedures, five figures, and two tables and can be found with this article online at doi:10.1016/j.cell.2010.02.039.

ACKNOWLEDGMENTS

ThromboGenics (TG) NV and BioInvent AB developed PlGF inhibitors for anti-angiogenic treatment under a license from VIB and K.U.Leuven. D.C. was the Founder and is Chairman of the Board of TG (indirectly holding 1% equity share); his participation relates to his scientific directorship of the VIB department (until October 2008) when most studies were ongoing. The research on anti-PlGF conducted in the lab of P.C. has been financed in small part by TG. This work was supported by K.U.Leuven, IUAP06/30, GOA2006/11, and Methusalem funding to P.C.; by LSHG-CT-2004-503573 to P.C., L.C.-W., and G. Christofori; by NCCR Molecular Oncology, Swiss Science Foundation to G. Christofori; by FWO G.0229.04 and G.0500.08, SCIE2006-3, and OT/08/37 to G. Carmeliet; by NIH grant CA69184, Swiss Science Foundation 3100A0-108207, and LSHC-CT-2005-518178 to M. Detmar; by NIH EY017164 to S.A.V.; by SAF 2007-63069 and 2009 SGR 1496 to M.M.-R.; by DFG fellowship to T.S.; and by DKH fellowship to S.L.

Received: December 23, 2009
Revised: February 5, 2010
Accepted: February 23, 2010
Published: April 1, 2010

REFERENCES

Bais, C., Wu, X., Yao, J., Yang, S., Crawford, Y., McCutcheon, K., Tan, C., Koluman, G., Vernes, J.-M., Easthma-Anderson, J., Haughney, P., et al. (2010). PlGF blockade does not inhibit angiogenesis during primary tumor growth. Cell *141*, this issue, 166–177.

Carmeliet, P., Dor, Y., Herbert, J.M., Fukumura, D., Brusselmans, K., Dewerchin, M., Neeman, M., Bono, F., Abramovitch, R., Maxwell, P., et al. (1998). Role of HIF-1alpha in hypoxia-mediated apoptosis, cell proliferation and tumour angiogenesis. Nature *394*, 485–490.

Carmeliet, P., Moons, L., Luttun, A., Vincenti, V., Compernolle, V., De Mol, M., Wu, Y., Bono, F., Devy, L., Beck, H., et al. (2001). Synergism between vascular endothelial growth factor and placental growth factor contributes to angiogenesis and plasma extravasation in pathological conditions. Nat. Med. *7*, 575–583.

Davidoff, A.M., Nathwani, A.C., Spurbeck, W.W., Ng, C.Y., Zhou, J., and Vanin, E.F. (2002). rAAV-mediated long-term liver-generated expression of an angiogenesis inhibitor can restrict renal tumor growth in mice. Cancer Res. *62*, 3077–3083.

Dawson, M.R., Duda, D.G., Chae, S.S., Fukumura, D., and Jain, R.K. (2009). VEGFR1 activity modulates myeloid cell infiltration in growing lung metastases but is not required for spontaneous metastasis formation. PLoS ONE *4*, e6525.

Dupuy, E., Hainaud, P., Villemain, A., Bodevin-Phedre, E., Brouland, J.P., Briand, P., and Tobelem, G. (2003). Tumoral angiogenesis and tissue factor expression during hepatocellular carcinoma progression in a transgenic mouse model. J. Hepatol. *38*, 793–802.

Fernandez, M., Semela, D., Bruix, J., Colle, I., Pinzani, M., and Bosch, J. (2009). Angiogenesis in liver disease. J. Hepatol. *50*, 604–620.

Fischer, C., Jonckx, B., Mazzone, M., Zacchigna, S., Loges, S., Pattarini, L., Chorianopoulos, E., Liesenborghs, L., Koch, M., De Mol, M., et al. (2007). Anti-PlGF inhibits growth of VEGF(R)-inhibitor-resistant tumors without affecting healthy vessels. Cell *131*, 463–475.

Fischer, C., Mazzone, M., Jonckx, B., and Carmeliet, P. (2008). FLT1 and its ligands VEGFB and PlGF: drug targets for anti-angiogenic therapy? Nat. Rev. Cancer *8*, 942–956.

Gerber, H.P., Wu, X., Yu, L., Wiesmann, C., Liang, X.H., Lee, C.V., Fuh, G., Olsson, C., Damico, L., Xie, D., et al. (2007). Mice expressing a humanized form of VEGF-A may provide insights into the safety and efficacy of anti-VEGF antibodies. Proc. Natl. Acad. Sci. USA *104*, 3478–3483.

Gordon, M.S., Margolin, K., Talpaz, M., Sledge, G.W., Jr., Holmgren, E., Benjamin, R., Stalter, S., Shak, S., and Adelman, D. (2001). Phase I safety and pharmacokinetic study of recombinant human anti-vascular endothelial growth factor in patients with advanced cancer. J. Clin. Oncol. *19*, 843–850.

Hawighorst, T., Velasco, P., Streit, M., Hong, Y.K., Kyriakides, T.R., Brown, L.F., Bornstein, P., and Detmar, M. (2001). Thrombospondin-2 plays a protective role in multistep carcinogenesis: a novel host anti-tumor defense mechanism. EMBO J. *20*, 2631–2640.

Hiratsuka, S., Nakamura, K., Iwai, S., Murakami, M., Itoh, T., Kijima, H., Shipley, J.M., Senior, R.M., and Shibuya, M. (2002). MMP9 induction by vascular endothelial growth factor receptor-1 is involved in lung-specific metastasis. Cancer Cell *2*, 289–300.

Ho, M.C., Chen, C.N., Lee, H., Hsieh, F.J., Shun, C.T., Chang, C.L., Lai, Y.T., and Lee, P.H. (2006). Placenta growth factor not vascular endothelial growth factor A or C can predict the early recurrence after radical resection of hepatocellular carcinoma. Cancer Lett. *250*, 237–249.

Johnson, S.J., Burr, A.W., Toole, K., Dack, C.L., Mathew, J., and Burt, A.D. (1998). Macrophage and hepatic stellate cell responses during experimental hepatocarcinogenesis. J. Gastroenterol. Hepatol. *13*, 145–151.

Landgren, E., Schiller, P., Cao, Y., and Claesson-Welsh, L. (1998). Placenta growth factor stimulates MAP kinase and mitogenicity but not phospholipase C-gamma and migration of endothelial cells expressing Flt 1. Oncogene *16*, 359–367.

Lassen, U., Nielsen, D., Sorensen, M., Ronnengart, E., Eldrup, K., Bentzon, K., Winstedt, L., Niskanen, T., Stenberg, Y., Pakola, S., et al. (2009). A phase I, dose escalation study of TB-403, a monoclonal antibody directed against PlGF, in patients with solid tumors. Mol. Cancer Ther. *8*, A111.

Loges, S., Mazzone, M., Hohensinner, P., and Carmeliet, P. (2009). Silencing or fueling metastasis with VEGF inhibitors: antiangiogenesis revisited. Cancer Cell *15*, 167–170.

Luttun, A., Brusselmans, K., Fukao, H., Tjwa, M., Ueshima, S., Herbert, J.M., Matsuo, O., Collen, D., Carmeliet, P., and Moons, L. (2002a). Loss of placental growth factor protects mice against vascular permeability in pathological conditions. Biochem. Biophys. Res. Commun. *295*, 428–434.

Luttun, A., Tjwa, M., Moons, L., Wu, Y., Angelillo-Scherrer, A., Liao, F., Nagy, J.A., Hooper, A., Priller, J., De Klerck, B., et al. (2002b). Revascularization of ischemic tissues by PlGF treatment, and inhibition of tumor angiogenesis, arthritis and atherosclerosis by anti-Flt1. Nat. Med. *8*, 831–840.

Marcellini, M., De Luca, N., Riccioni, T., Ciucci, A., Orecchia, A., Lacal, P.M., Ruffini, F., Pesce, M., Cianfarani, F., Zambruno, G., et al. (2006). Increased melanoma growth and metastasis spreading in mice overexpressing placenta growth factor. Am. J. Pathol. *169*, 643–654.

Mazzone, M., Dettori, D., Leite de Oliveira, R., Loges, S., Schmidt, T., Jonckx, B., Tian, Y.M., Lanahan, A.A., Pollard, P., Ruiz de Almodovar, C., et al. (2009). Heterozygous deficiency of PHD2 restores tumor oxygenation and inhibits metastasis via endothelial normalization. Cell *136*, 839–851.

Nozawa, H., Chiu, C., and Hanahan, D. (2006). Infiltrating neutrophils mediate the initial angiogenic switch in a mouse model of multistage carcinogenesis. Proc. Natl. Acad. Sci. USA *103*, 12493–12498.

Oura, H., Bertoncini, J., Velasco, P., Brown, L.F., Carmeliet, P., and Detmar, M. (2003). A critical role of placental growth factor in the induction of inflammation and edema formation. Blood *101*, 560–567.

Paternostro, C., David, E., Novo, E., and Parola, M. (2010). Hypoxia, angiogenesis and liver fibrogenesis in the progression of chronic liver diseases. World J. Gastroenterol. *16*, 281–288.

Riisbro, R., Larsson, L., Winsted, L., Niskanen, T., Pakola, S., Stassen, J.M., Lassen, U., and Glazer, S. (2009). A first-in-man phase I dose escalation study of TB403, a monoclonal antibody directed against PlGF in healthy male subjects. Mol. Cancer Ther. *8*, A3.

Roncal, C., Buysschaert, I., Gerdes, N., Georgiadou, M., Ovchinnikova, O., Fischer, C., Stassen, J.M., Moons, L., Collen, D., De Bock, K., et al. (2010). Short-term delivery of anti-PlGF antibody delays progression of atherosclerotic plaques to vulnerable lesions. Cardiovasc. Res. *86*, 29–36. Published online December 28, 2009. 10.1093/cvr/cvp380.

Taylor, A.P., and Goldenberg, D.M. (2007). Role of placenta growth factor in malignancy and evidence that an antagonistic PlGF/Flt-1 peptide inhibits the

growth and metastasis of human breast cancer xenografts. Mol. Cancer Ther. *6*, 524–531.

Van Steenkiste, C., Geerts, A., Vanheule, E., Van Vlierberghe, H., De Vos, F., Olievier, K., Casteleyn, C., Laukens, D., De Vos, M., Stassen, J.M., et al. (2009). Role of placental growth factor in mesenteric neoangiogenesis in a mouse model of portal hypertension. Gastroenterology *137*, 2112–2124.

Willett, C.G., Boucher, Y., Duda, D.G., di Tomaso, E., Munn, L.L., Tong, R.T., Kozin, S.V., Petit, L., Jain, R.K., Chung, D.C., et al. (2005). Surrogate markers for antiangiogenic therapy and dose-limiting toxicities for bevacizumab with radiation and chemotherapy: continued experience of a phase I trial in rectal cancer patients. J. Clin. Oncol. *23*, 8136–8139.

Wittko, I.M., Schanzer, A., Kuzmichev, A., Schneider, F.T., Shibuya, M., Raab, S., and Plate, K.H. (2009). VEGFR-1 regulates adult olfactory bulb neurogenesis and migration of neural progenitors in the rostral migratory stream in vivo. J. Neurosci. *29*, 8704–8714.

Wu, X.Z., Xie, G.R., and Chen, D. (2007). Hypoxia and hepatocellular carcinoma: The therapeutic target for hepatocellular carcinoma. J. Gastroenterol. Hepatol. *22*, 1178–1182.

Xu, L., and Jain, R.K. (2007). Down-regulation of placenta growth factor by promoter hypermethylation in human lung and colon carcinoma. Mol. Cancer Res. *5*, 873–880.